Journal of Molecular Liquids 345 (2022) 118210

Contents lists available at ScienceDirect

Journal of Molecular Liquids

journal homepage: www.elsevier.com/locate/molliq

Molecular simulation studies of self-assembly for a chromonic perylene dye: All-atom studies and new approaches to coarse-graining

Gary Yu, Mark R. Wilson *

Department of Chemistry, Durham University, Science Laboratories, Lower Mountjoy, Stockton Road, Durham DH1 3LE, UK

ARTICLE INFO

Article history:
Received 10 August 2021
Revised 8 November 2021
Accepted 23 November 2021
Available online 27 November 2021

Keywords:
Chromonic liquid crystals
Coarse-grained modelling
Molecular dynamics

ABSTRACT

Perylene tetracarboxylic acid bisimides are compounds that show intense visible light absorption and exhibit excellent chemical, photochemical and thermal stability. As such, they have been widely used as dyes and have a range of industrial applications. These dyes have also been investigated for various applications in aqueous media as chromonic liquid crystals: lyotropic systems characterised by the association of aromatic mesogenic cores into stacked structures. In this study, we focus on one perylene dye bis-(N,N-diethylaminoethyl) perylene-3,4,9,10-tetracarboxylic diimide dihydrochloride, PER, and study its self-assembly in aqueous solution through both atomistic and coarse-grained molecular models. All-atom molecular dynamics simulations demonstrate spontaneous self-assembly into chromonic H-aggregate stacks with an interparticle twist between molecules. The coarse-graining of complex chromonic mesogens introduces a wealth of subtle complexities that presents a significant challenge to overcome. Consequently, we developed coarse-grained (CG) models using both bottom-up and top-down approaches: the multiscale coarse-graining method (MS-CG) in the form of hybrid force matching (FM) and the MARTINI 3 force field, respectively. We discuss the successes/deficiencies of these approaches and introduce changes to improve upon their performance and representability. For the MARTINI 3 model, careful optimisation of parameters allows it to exactly reproduce the atomistic self-assembly behaviour including the relevant thermodynamic properties in solution. The bottom-up CG model, produced using a conventional MS-CG treatment, fails to reproduce most of the target properties, but the implementation of the potentials into a combined FM-MARTINI 3 framework allows the recovery of the correct self-assembly behaviour in solution.

1. Introduction

Perylene tetracarboxylic acid bisimides have been widely used as stable dyes in industrial applications and have also received considerable attention in academic research [1]. The syntheses and functionalisation of perylene dyes, their applications in organic photovoltaic materials and a plethora of supramolecular architectures with numerous modes of organisation have been extensively reported in the literature [2–5]. Subsequently, perylene dyes and analogues have been designed and investigated for various applications in aqueous media as chromonic liquid crystals [6–11]. Chromonics are an unusual class of lyotropic liquid crystals, where aggregates are characterised by the intermolecular association of aromatic cores into stacked structures [12]. In this study, we focus on one perylene dye, bis-(N,N-diethylaminoethyl)perylene-3,4,9,10-tetracarboxylic diimide dihydrochloride, which will be known as PER throughout. Studies on PER show that it forms stacks of H-aggregate character which organise into a chromonic nematic phase at room temperature (with a hexagonal phase at higher concentrations) [13,14]. The stacks are indicated to be one molecule wide, assemble in an isodesmic fashion and have a free energy change of 16–20 k_BT for the removal of a molecule from a stack [15]. X-ray diffraction reveals a peak corresponding to an intra-column spacing of 0.3–0.4 nm, where its broadness is attributed to disordered stacking [13]. The thermodynamics of the aggregation have also been characterised for various derivatives of PER by simulation and experiment, with the effects of solvent, temperature and substituents explored [16–18].

Molecular dynamics simulations (MD) have been extensively applied to study aggregation in aqueous solutions. At the all-atom (AA) level, detailed insights on the nature of the self-assembly, association thermodynamics, arrangement of molecules in aggregates and the interplay between structures can be acquired for chromonics [19–26,16–18,27–29]. While AA MD provides a powerful way of understanding these systems, the study of chro-

* Corresponding author.
E-mail address: mark.wilson@durham.ac.uk (M.R. Wilson).

https://doi.org/10.1016/j.molliq.2021.118210
0167-7322/

monic liquid crystal phases and complex large-scale aggregates is limited by the computational efficiency of atomistic simulation. For example, timescales for self-assembly and self-organisation of aggregates can extend well beyond the μs regime, i.e. well beyond times currently accessible for atomistic studies. However, coarse-graining, where groups of atoms are represented by single sites, offers a route to simulating systems beyond the length and time scales accessible to AA MD. Using a simplified lower-resolution representation allows for the number of particles present to be reduced, a larger time step to be used and more efficient movement through a simplified phase space [30].

The non-ionic chromonic, TP6EO2M, has proved an interesting test bed for the development of coarse-grained (CG) models of self-assembly in solution, and a number of different resolution CG models have been developed, which have facilitated the study of its mesophase behaviour [31–34]. At the simplified level of dissipative particle dynamics (DPD), the full chromonic phase diagram has been explored with the nematic (N) and hexagonal (M) phases being observed, and an exponential distribution of stack sizes obtained in the isotropic phase [31]. Variants of this DPD model predict an array of novel structures and phases with complex stacks of two and three molecule cross-sections [32]. The effectiveness of systematic coarse-graining methods have also been investigated to develop more chemically specific CG models for TP6EO2M; revealing a range of challenges in the coarse-graining of chromonic liquid crystals and the self-assembly process [33,34]. A subtle balance of hydrophobic-hydrophilic interactions within the molecules must be achieved for chromonic self-assembly to occur. In addition, considerations in the mapping and association strengths between the mesogens themselves (and with water) are pertinent to the success of the CG model.

In this study, we build upon the existing work for TP6EO2M and explore bottom-up and top-down coarse-graining methods for the cationic perylene-core dye, PER. PER and similar chromonic systems provide enhanced challenges for coarse-grained modelling because of their ionic nature, an increase in the number of different regions within the molecule (in comparison to molecules like TP6EO2M), and an extended anisotropic aromatic region.

The organisation of this paper is as follows. Firstly, we present atomistic MD simulation work on PER. We demonstrate spontaneous aggregation in water to form chromonic H-aggregates that exhibit an interlayer twist between molecules; and we quantify the self-assembly behaviour in terms of thermodynamic quantities: the free energy of aggregation and the hydration free energy. Secondly, we apply the bottom-up multiscale coarse-graining (MS-CG) method [35], in the form of hybrid force matching (FM) [36,37], to parametrise CG models based on AA reference data. Here, multiple strategies are assessed but none result in a completely satisfactory CG model in terms of the solution self-assembly. Thirdly, we construct a top-down CG model using the MARTINI 3 framework [38] and show that a simple optimisation of this model allows for the exact reproduction of the relevant thermodynamic properties and the solution self-assembly. Finally, we demonstrate that a combined approach between FM and MARTINI can improve upon the deficiencies of standard FM CG models.

2. Computational Methods

2.1. Simulation details

The General AMBER Force Field (GAFF) was employed for all atomistic simulations [39]. The Antechamber package from AmberTools18 [40] was used to generate Lennard-Jones (LJ) potentials and partial charges for the force field, with the latter employing the AM1-BCC method [41]. The resulting GAFF topologies were converted into the necessary input files for GROMACS using the ACPYPE script [42]. All simulations used the TIP3P water model [43], which has been used in the development of GAFF [44]. All MD simulations were carried out using the GROMACS 2018.7 molecular dynamics simulation package [45]. The Particle Mesh Ewald (PME) method was used to handle long-range electrostatics, with a cut-off of 1.2 nm used for all short-range interactions [46]. After minimisation, a 100 ps pre-equilibration run in the *NVT* ensemble was carried out using a modified Berendsen thermostat followed by a 100 ps pre-equilibration in the *NpT* ensemble with the addition of the Berendsen barostat [47]. An equilibration run of 200 ps and a subsequent production simulation for 500 ns utilised the Nosé-Hoover thermostat [48,49] to maintain a constant temperature of 300 K, and the Parrinello-Rahman barostat [50] to keep the pressure constant at 1 bar. A leap-frog algorithm was employed with a time step of 1 fs for equilibration with an increase to 2 fs for production runs, where constraints were implemented using the Linear Constraints Solver (LINCS) method [51].

Coarse-grained simulations were performed using a 2 fs time step for initial equilibration and 5 fs for production runs, where the length of each stage follows the atomistic conditions, as stated above. CG simulations did not employ bond constraints. The same thermostats, barostat and cutoffs used for AA MD were also employed for all FM CG models. The MARTINI 3 CG models used a reduced cutoff of 1.1 nm for all interactions and a dielectric constant $\epsilon_r = 15$, as used in the development of the MARTINI 3 framework [52]. The standard MARTINI 3 simulation conditions were employed, using the modified velocity rescaling thermostat in GROMACS 2018 [53] and the reaction-field method for electrostatics [54] (where $\epsilon_{rf} = \infty$ beyond the cutoff).

2.2. Coarse-grained mapping

The interaction site for a coarse-grained bead is defined by the centre of mass (COM) of its constituent atoms as follows

$$\boldsymbol{R}_I = \sum_i^n \left(\frac{\boldsymbol{r}_i m_i}{\sum_i^n m_i} \right), \tag{1}$$

where $\boldsymbol{R}_I$ is the position of CG bead I, $\boldsymbol{r}_i$ and m_i are the position and mass of an atom i, respectively, and n is the number of atoms contained in the CG bead. In this work, we use a single mapping scheme for all CG models of PER with a mapping of 2/3 heavy atoms to a bead for the aromatic core, 5 heavy atoms for the imide group, 2 heavy atoms for the connecting ethyl group and 5 heavy atoms for the terminal diethylammonium group (where all beads also contain the associated hydrogen atoms). For FM CG systems, water and chloride ions are mapped in a 1:1 fashion whereas, for MARTINI 3, we use the standard 4:1 mapping for water. Overall, this mapping leads to a total of 6 bead types (4 for PER and 2 for the solvent) and 21 pairwise, non-bonded interaction potentials to be parametrised.

The bonded parameters are parametrised separately using probability distributions generated from a single-molecule AA MD trajectory of PER in TIP3P water. From each distribution, equilibrium bond lengths, angles and dihedrals were defined as the value of the maximum probability. These were then implemented as harmonic potentials with appropriate force constants chosen. Improper dihedral potentials were applied to the aromatic core to ensure planarity. All CG models in this work employed the same set of bonded parameters (see ESI Figure S1 and Tables S1–3). (Figs. 1 and 2).

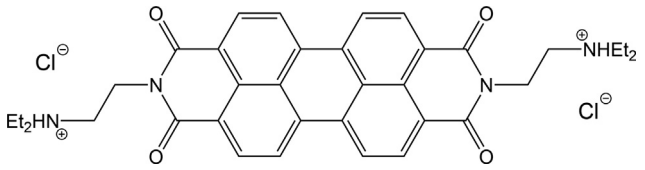

Fig. 1. Molecular structure of PER with its counterions.

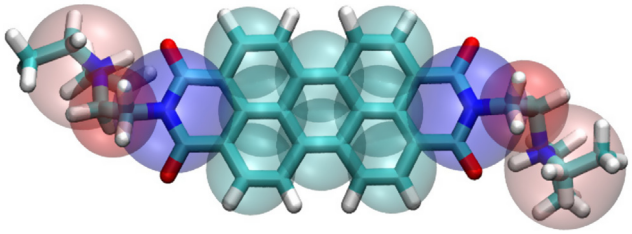

Fig. 2. Coarse-grained mapping scheme for PER.

2.3. Multiscale coarse-graining

The multiscale coarse-graining (MS-CG) method [35] is a force-based method, extended into the framework of coarse-graining from the force matching method [55]. The idea is to match force distributions obtained from the reference atomistic model to forces acting between CG sites. The theoretical basis from statistical mechanics has, subsequently, been derived and reported [56–58]. The variational principle derived is given by

$$\chi^2 = \frac{1}{3LN}\sum_{l=1}^{L}\sum_{i=1}^{N}\left|\boldsymbol{F}_{il}^{\mathrm{AA}} - \boldsymbol{F}_{il}^{\mathrm{CG}}(x_1,\ldots,x_M)\right|^2, \tag{2}$$

where χ^2 is the objective function be to minimised, L and N are the total number of snapshots and particles, respectively, $\boldsymbol{F}_{il}^{\mathrm{AA}}$ and $\boldsymbol{F}_{il}^{\mathrm{CG}}$ are the total force on bead i in snapshot l for the AA and CG systems, respectively, and $x_1,\ldots,x_M$ are coefficients for fitting.

Here, the hybrid force matching (FM) approach has been implemented: bonded potentials are obtained separately, and the non-bonded potentials are calculated by the MS-CG method [37,36]. An extension of this is used here to separate out the electrostatic contributions so that they may be explicitly treated in the simulation with the PME method. This was achieved by an additional step in which CG electrostatic forces, from the mapped atomistic charges, were subtracted from the effective, mapped reference trajectory before the MS-CG method was applied [34]. Charges for each CG bead are obtained by summing up the atomic charges of its constituent atoms.

MS-CG was carried out using the BOCS (Bottom-up Open-source Coarse-graining Software) package [59]. Reference trajectories for this method contained 1000 snapshots from a 10 wt% system of 15 molecules, for which intramolecular forces were excluded. We present 2 different FM CG models, which differ in the reference trajectories used in their parametrisation: i) a 10 ns simulation of a self-assembled system containing stacks of tetramer size and above and ii) a longer reference simulation (100 ns) which captures self-assembly from a dispersed system of monomers into dimers and then tetramers. The finer details of these CG models will be presented in Section 3.2. The potentials obtained are given in the ESI (Figures S2–22).

CG potentials constructed with this methodology overestimate the pressure of the system and, thus, require a pressure correction to allow for simulation in the *NpT* ensemble at 1 bar with the correct density. Here, we adopt an approach previously applied to FM potentials [60,34], via the VOTCA-CSG (Versatile Object-oriented Toolkit for Coarse-graining Applications) package, version 1.4.1 [61,37,62]. A linear pressure correction was applied, in an iterative manner, to all the potentials simultaneously as follows

$$\Delta U(r) = A\left(1 - \frac{r}{r_{\mathrm{cut}}}\right) \tag{3}$$

where

$$A = \mathrm{sgn}(\Delta P)0.1k_{\mathrm{B}}T\ \ \min\left(1, |f\Delta P|\right). \tag{4}$$

In these equations, r_{cut} is the cut-off distance, ΔP is the difference in pressure between the reference and coarse-grained system and f is a scaling factor. It should be noted that this correction does not strictly address the state-point dependence of the potentials, which requires additional terms in the coarse-graining procedure relating to volume/density dependent components [63–65].

2.4. MARTINI 3

The MARTINI force field is a popular top-down coarse-graining approach in which building blocks are parametrised to reproduce partitioning behaviour between aqueous–hydrophobic environments, and was originally produced for lipid/membrane simulation but has been extended to a range of systems [66–68]. MARTINI consists of a library of CG beads whose potentials have been extensively calibrated against thermodynamic data with the aim of high transferability. Thus, the resulting beads can be used in a broad range of systems at various thermodynamic state points without the need to reparametrise each time. These particles interact via Lennard-Jones 12:6 potentials.

In this work, we use the new MARTINI 3 force field, which provides more subtypes for different levels of coarse-graining in comparison to the earlier incarnation [38]. It is noted that this study was conducted prior to the formal publication of MARTINI 3, and so uses the parameters released in the open beta version [69]. The bead types selected for the CG model will be discussed in Section 3.3.

2.5. Free energy of association

The free energy of association, $\Delta G_{\mathrm{assoc}}$, for a n-mer can be determined from a potential of mean force (PMF), where the PMF describes the work done to pull two species apart. This PMF is calculated from a series of simulations in which the pulled species are constrained at specified points over a separation distance. The PMF, U_{PMF}, is then obtained by integrating the average constraint force, $\langle f_{\mathrm{c}}\rangle_s$, over the separation distance, s, according to the equation

$$U_{\mathrm{PMF}}(r) = \int_{r}^{r_{\max}}\left[\langle f_{\mathrm{c}}\rangle_s + \frac{2k_{\mathrm{B}}T}{s}\right]ds, \tag{5}$$

where r is the distance, $r_{\max}$ is the maximum distance and $2k_{\mathrm{B}}T/s$ is a kinetic entropy term which accounts for the increase in rotational volume at larger separation distances [70–72].

PMFs were calculated for systems at a concentration of 1 wt%, where a pull was administered between the COMs of each species with a pull rate of 0.001 nm ps^{-1}. Configurations along this pull were extracted with neighbouring points varying from 0.02–0.1 nm between windows. Each window was equilibrated for 1 ns before sampling for 20 ns in a production run. A total of 1×10^6 force values were obtained for each window along the separation distance and used to calculate the average constraint force before integration to obtain the PMF.

2.6. Free energy of hydration

The Bennett acceptance ratio (BAR) method can be used to calculate the free energy difference (ΔF_{BA}) between two states, A and B [73]. Multiple intermediate states are defined by a coupling parameter, λ, and a Hamiltonian, H, is calculated for each state. The free energy difference between states i and j can then be evaluated according to

$$\Delta F_{ji} = k_B T \ln \frac{\langle f(H_i - H_j + C)\rangle_j}{\langle f(H_j - H_i + C)\rangle_i} + C, \tag{6}$$

where

$$f(x) = \frac{1}{1 + \exp(x/k_B T)}. \tag{7}$$

The value of the constant, C, is numerically determined to fulfil $\langle f(H_i - H_j + C)\rangle_j = \langle f(H_j - H_i + C)\rangle_i$. The total free energy difference is calculated as the sum of all intermediate free energy differences,

$$\Delta F_{BA} = \sum_{i=1}^{n-1} \Delta F_{i+1,i}. \tag{8}$$

When decoupling interactions, particles may get very close to each other (near the end points when the interactions are weak) and cause large fluctuations in the potential energy. This problem can be circumvented by using soft-core potentials given by

$$U_{SC}(r) = (1 - \lambda)U_A(r_A) + \lambda U_B(r_B) \tag{9}$$

$$r_A = (\alpha\sigma_A^6 \lambda^p + r^6)^{\frac{1}{6}} \tag{10}$$

$$r_B = (\alpha\sigma_B^6 (1 - \lambda)^p + r^6)^{\frac{1}{6}}, \tag{11}$$

where α is the soft-core parameter (0.5), σ is the radius of the interaction and p is a positive integer (1).

Free energies of hydration, ΔG_{hydr}, were calculated by decoupling the intermolecular interactions of a single molecule from the solvent at a concentration of 0.5 wt%, where the hydration of the species is the reverse of this process. Coulombic interactions were first decoupled linearly before the van der Waals interactions with a total number of 41 states of λ between 0 and 1, with a spacing of 0.05. Simulations for each λ state consisted of a 1 ns equilibration followed by a 5 ns production run for data collection.

2.7. Twist angle analysis

For neighbouring molecules in a stacked structure, a twist angle can be defined as

$$\theta = \cos^{-1}(v_i . v_j), \tag{12}$$

where v_n is the unit vector defined by

$$v_n = L_n \times d_n. \tag{13}$$

θ is the twist angle and L_n is the direction vector for molecule n. The atoms used to define this vector were the two nitrogen atoms of the imide groups in the core.

3. Results and Discussion

3.1. Atomistic Simulations

Atomistic molecular dynamics simulations were performed on a 10 wt% system consisting of 15 molecules of PER. These allowed for the self-assembly behaviour to be observed and the calculation of structural and thermodynamic properties, from which we can inform and validate the resultant CG models.

Fig. 3(a) shows the PMF for a PER dimer, from which the free energy of association is calculated to be -47 ± 3 kJ mol^{-1} (18.7 $k_B T$) at a favoured COM distance of 0.39 nm. Errors in ΔG_{assoc} are calculated by propagation from each data point used in the PMF calculation and the error for ΔG_{hydr} (below) is estimated from block averaging. Because PER is a di-cation and also contains an extended aromatic π-system, the value obtained for ΔG_{assoc} is appreciably higher than previously calculated values for anionic and non-ionic chromonics (7–15 $k_B T$ [20–22,19]). However, the calculated value is within the range determined experimentally for this dye (16–20 $k_B T$) [15]. Configurations extracted from the minimum of the PMF (Fig. 3(b)) correspond to H-aggregate behaviour (direct stacking) with a small twist between the molecules to reduce steric/electrostatic repulsion between the bulky, charged end groups. The free energy of hydration obtained is -133 ± 1.0 kJ mol^{-1}, indicating the soluble nature of this dye in aqueous solution.

The self-assembly into stacks from a random configuration of dispersed monomers occurs rapidly, with few species below trimer size present within 50 ns. Over several hundred nanoseconds, large stacks form and continuously break apart and reform as observed previously in simulations of ionic chromonic dyes [19]. A typical stack is shown in Fig. 3c) and displays a one molecule width cross-section and an interlayer twist between molecules going along the stack; both properties are observed in experiment [3,15]. We note that a periodic twist in a single direction along the stack is not observed, and so the interlayer angular offset between adjacent molecules does not impart chirality upon the aggregates. From further analysis of the twist angle (Fig. 3(d)) between adjacent molecules in a stack, we see a preference for rotations of 6°, 24°, 156° and 174°.

3.2. Force Matching

Using the MS-CG method, three bottom-up coarse-grained models of PER were developed via hybrid force matching. The first was a neutral (i.e. uncharged) FM model (FM-N), where electrostatic contributions in the AA reference system were incorporated into the effective pair potentials constructed by the MS-CG method. This model assumes the long-range contributions from charges are screened completely by counter-ions and water. Hence, simulations of the FM-N model used no partial charges on any beads. The model was parametrised using an AA trajectory for a system of 15 PER molecules and counterions at 10 wt% in water. The reference system dynamically consisted of two or three stacks, which varied in aggregation number through the trajectory. The second (and principal) CG model (FM1) to be considered in this work used the same reference trajectory but utilised partial charges on beads arising from the AA model and treated them explicitly. This methodology was expected to improve the representability of the ionic nature of the dye compared to a neutral version. A second FM model, which also has partial charges present, was constructed with a longer AA reference trajectory (FM2) that started from 15 dispersed monomers and generated a range of dimers, trimers and tetramers through the trajectory. A schematic representation of the mapping in these FM models is shown in Fig. 4(a). It is noted that the partial charges for C beads are only present on the four outer beads of the core. The FM models developed here provide a considerable computational speed up compared to the all-atom model, through a mixture of an increase in timestep, reduction in the number of sites and an accelerated exploration of phase space.

The free energies of association and hydration for each model are summarised in Table 1 and PMF profiles are shown in Fig. 4 (b). The binding energies for all three FM models are much higher

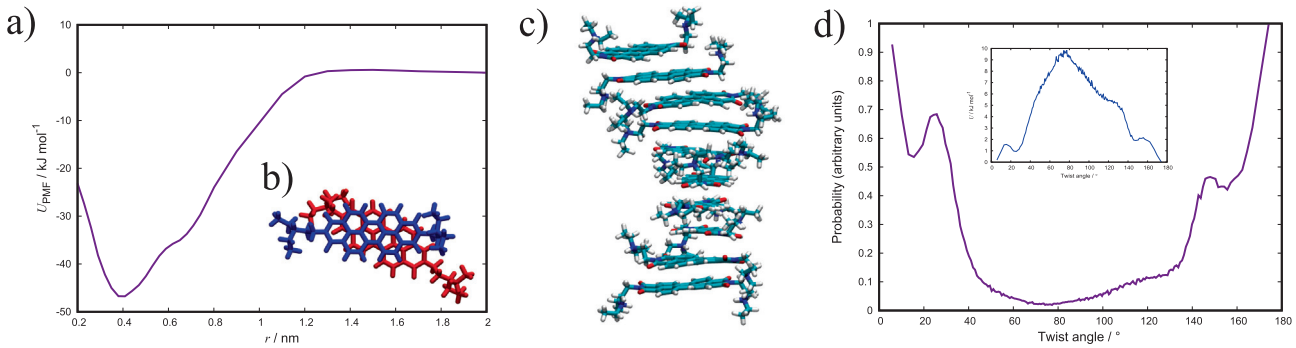

Fig. 3. (a) PMF for a dimer of PER in TIP3P water at 300 K with a (b) top-down view of a dimer configuration showing an interlayer twist. (c) A simulation snapshot of a 10 molecule stack of PER extracted from a 10 wt% system of 15 molecules. (d) Histogram of the twist angle between neighbouring molecules with the inset showing the corresponding potential.

than the target AA value; a trait observed previously for CG models of chromonics generated by force matching [34]. The PMFs appear to have ill-defined wells, compared to the atomistic system, which indicates that configurations of the dimer throughout the reaction coordinate are relatively favourable; with the minimum of the PMF occuring at a COM distance of 0.35 nm, which is noticeably shorter than expected. This may arise due to a number of reasons: i) the FM potentials are not of a fixed form and are generally softer than typical 12:6 LJ potentials, which allows for a greater degree of overlap, ii) imbalances between interactions on the peripheral beads could result in increased torsions manifesting as a distortion in the dimer configuration (where it is noted that the orientation of the end groups affects the COM of molecule) and iii) the high attraction/hydrophobicity of the model results in close configurations to be prefered, even if they are strained. The hydration free energies (with the exception of FM2) are all of the wrong sign and suggests that the models are insoluble in water. The association strength of a dimer can be said to depend on two factors: the attractive interactions between the molecules and the extent of solubility of the monomers. Thus, we can rationalise the trend in association free energies across the models with the magnitude/sign of the hydration free energies. As the solubility of the model decreases, the binding energy increases through the range.

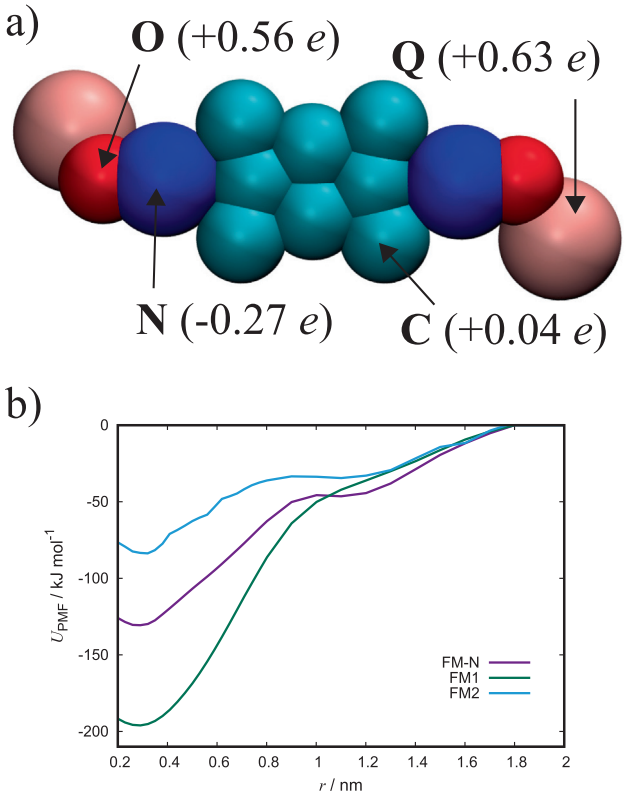

Fig. 4. (a) Schematic diagram showing the mapping used for the FM coarse-grained models, with the definition of bead types and their partial charges. (b) PMFs for a dimer of each FM CG model.

Simulations of the three FM models all produced the same type of self-assembly; a single aggregate forming in solution. However, while some face-to-face stacking of molecules was seen within the aggregate, the single-molecule cross-section chromonic stacks (seen atomistically) were not observed. Snapshots of this aggregate structure are presented in Fig. 5 for the FM1 model; noting that the other models form aggregates that are visually indistinguishable. The behaviour can be explained by the unfavourable combination of large attractive interactions between the solutes and the insolubility of the aggregates, which provides a strong driving force for phase separation. The influence of cross interactions between components of the chromonic species and water on the morphology of aggregates has been discussed previously by Potter and co-workers [33]. The authors report that a subtle balance of interactions is required to obtain chromonic behaviour: if association strength is too low, no chromonic stacks are seen; if association strength is too high insoluble aggregates form; if there is an incorrect balance of hydrophilic-hydrophobic interactions between parts of the molecule and water (i.e. the hydrophilic N, O, Q beads and hydrophobic C beads in this model) then aggregates form readily but without chromonic stacking.

The FM-N model can be considered the vanilla model where any short-range electrostatic effects are assumed to be correctly captured in the CG potentials and any long-range electrostatic effects are assumed to be screened out. However, this effectively averages the electrostatic forces over all the beads and neglects the ionic nature of the dye. Whereas in the FM1-2 models, partial charges can explicitly interact and affect the attraction/repulsion between beads. Interestingly, and regardless of charge treatment, the FM models have two interaction potentials that dominate their behaviour: the CC and CW interactions (Figure S2 and S11, respec-

Table 1
Free energies of association (ΔG_{assoc}) and hydration (ΔG_{hydr}) for the various FM models.

Model	FM-N	FM1	FM2
ΔG_{assoc}/ kJ mol^{-1}	−131 ± 3	−195 ± 2	−84 ± 4
ΔG_{hydr}/ kJ mol^{-1}	+85.8 ± 0.6	+130.2 ± 0.18	−79.9 ± 0.4

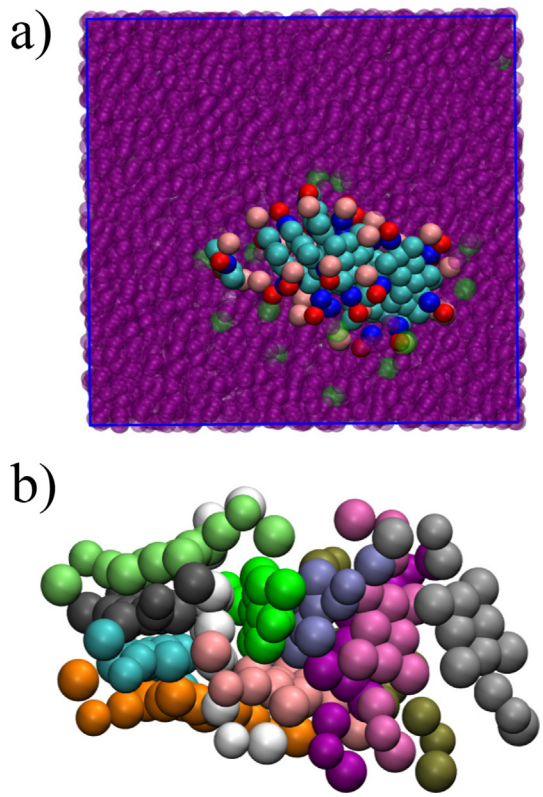

Fig. 5. (a) A simulation snapshot from a 10 wt% system of 15 molecules for the FM1 model, where the purple and green beads represent water and chloride ions, respectively. (b) A focused view of the aggregate with individual molecules coloured differently and the solvent removed for visual clarity.

tively); although other pair interactions do contribute to a lesser extent to molecular association and the hydration free energy. The CC interaction differs between FM-N and FM1, where the position of the well is identical but the strength of the FM1 CC interaction is 1.5 kJ mol^{-1} greater than for FM-N. The CW potentials are almost identical between these two models, as the separation of electrostatics from the FM potentials should have minimal effect on neutral beads. Therefore, we expect the FM1 model to have a greater association strength than FM-N, and this is indeed the case. Despite the difference in the thermodynamic quantities calculated for both these models, it is difficult to declare whether one is more successful than the other as both fail to properly represent the molecular association behaviour seen atomistically. We suggest that the poor representation of the solubility produces incorrect aggregation, and this arises from i) a lack of screening effects from the fully neutral CG water, ii) solute–solvent interactions which are not favourable enough and iii) an emphasis on reproducing structure in the MS-CG procedure rather than thermodynamic properties.

In order to improve representability, we tested the parametrisation process on a different AA reference trajectory. The justification for this approach arises from the assumption that a reference system containing just large stacks will produce CG potentials that seek only to reproduce the observed behaviour, neglecting the existence of smaller species and the solubility of monomers in solution. The FM2 model is based on a long reference trajectory, which captures the full self-assembly process from a dispersed system of monomers to small stacks, and provides a much richer ensemble of configurations than the initial reference. In essence, this is similar to a multi-state approach to coarse-graining which employs an ensemble of references at different state points to improve the transferability of the resulting model [59,74,75]. However, as mentioned above, simulations with the FM2 model do not produce the correct aggregation behaviour, although it does produce aggregates that are slightly less dense that those seen for model FM1. The FM2 model shows increased solute–water interaction strengths and weaker/similar solute–solute interaction strengths compared to the FM1 model. It is noted that the FM2 model does not produce the double-well potential typically seen for CG water [76], whereas the FM-N and FM1 models do (Figure S6). This may arise from the dynamic nature of the solutes in the FM2 reference disrupting the longer range water-water interactions. The increased hydrophilicity of this model originates from the aromatic region of the molecules experiencing a solvated environment for a significant period in the reference trajectory before being shielded by the formation of stacks. Overall, this model shows an improvement over the FM1 and FM-N models across the range of assessment criteria with FM2 even showing solubility in water. However unfortunately, this model cannot be deemed to have greater success in simulating chromonic self-assembly. It seems that there is a fundamental issue in representing the correct aqueous behaviour in FM CG models, which limits their ability to form discrete, soluble stacks. A future way of addressing this may be by the incorporation of local density potentials [65,77–79], which could allow for the local density of water to be captured around a given bead depending on the status of the molecule as a monomer, or its position in the centre/end of a stack.

3.3. MARTINI

An initial MARTINI 3 coarse-grained model was constructed using the recommended bead types (the details of the parameters can be found elsewhere [38,69]) for each chemical group present, as seen in Fig. 6(a). Simulation of this CG model and visual inspection showed that it produced self-assembly behaviour that was in good agreement with the AA system. Simulations of this model were 25x faster than the AA system, in addition to speeds ups arising from a faster exploration of phase space. (Noting that, the faster dynamics of these models should therefore not be directly compared to experiment.) The free energy of association and hydration were calculated to be -22 ± 2 kJ mol^{-1} (at a favoured COM distance of 0.39 nm) and -101.8 ± 0.5 kJ mol^{-1}, respectively. While both these free energies are lower than for the AA model, the correct self-assembly is captured well; demonstrating a favourable balance between the competing hydrophilic and hydrophobic interactions that are required to result in chromonic self assembly. Nonetheless, we can exert a degree of control on the binding energy of the model by using different MARTINI bead types to represent the core of the molecule. For example, Fig. 6(b) summarises the effect of varying the two bead types present in the core (from n = 1 to 5 for both TCn and Pn), where the trends obtained are, as expected, in line with increasing the hydrophobicity or polarity of the components. It is noted that this also varies the hydration free energies of the model.

Using the insights from Fig. 6(b), we can obtain even finer control on the thermodynamic properties by tuning MARTINI 3 LJ interactions for the core–water and core–core beads. Here, we optimise the TC4–WN interaction strength to reproduce the AA hydration free energy before optimising the TC4–TC4 interaction strength to reproduce the AA binding energy. By only using one pair potential to optimise each thermodynamic property, a linear relationship between the LJ well depth and the magnitude of the respective free energy is obtained. Thus, we developed a custom bead type, TCp, where ϵ(TCp–WN) = 1.945 kJ mol^{-1} and ϵ(TCp–TCp) = 2.998 kJ mol^{-1}, and σ for both potentials is unchanged. For comparison, the original MARTINI parameters were ϵ(TC4–WN) = 1.19 kJ mol^{-1} and ϵ(TC4–TC4) = 1.45 kJ mol^{-1}. A MD simu-

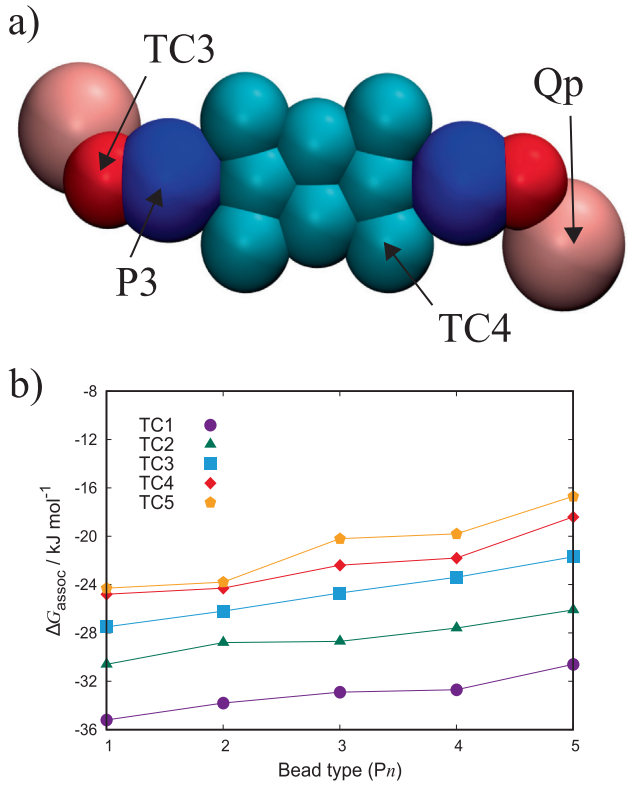

Fig. 6. (a) Schematic diagram for the MARTINI 3 coarse-grained model (M3) showing the bead types used. Water is modelled using the WN bead type and chloride ions are represented by TQ1 beads. (b) ΔG_{assoc} as a function of varying bead types for the core. TCn, in the key, refers to the inner core beads and Pn, on the x-axis, denotes the outer core beads.

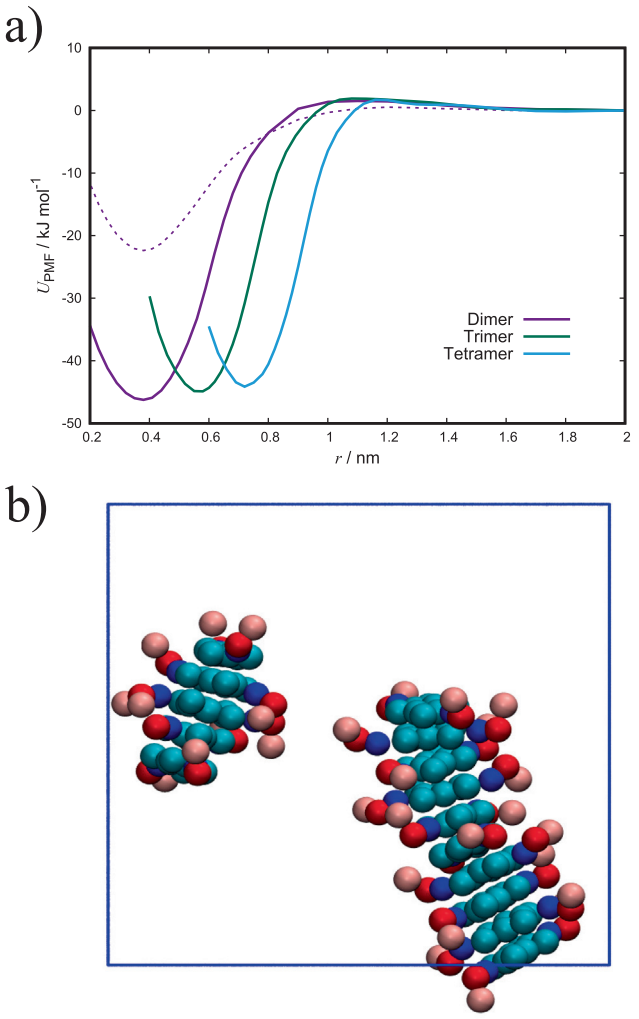

Fig. 7. (a) PMFs for a dimer, trimer and tetramer of the optimised M3 model, where the dashed curve corresponds to the initial M3 model. (b) A simulation snapshot from a 10 wt% system of 15 molecules.

lation of this optimised M3 model shows that the same self-assembly behaviour as the AA model is displayed (Fig. 7(b)), as captured by the initial MARTINI 3 model, but now the optimised version exactly captures the target thermodynamic properties.

In addition to the dimer PMFs, we can calculate profiles for trimers and tetramers to compare association of a monomer to stacks of differing size (Fig. 7(a)). Sampling of forces was performed between the COM of the stack and the pulled molecule, resulting in a shift of the PMF minima compared to the dimer. We observe that aggregation here is isodesmic as the binding energies of a dimer, trimer and tetramer are approximately the same. Chromonic systems are generally considered isodesmic, where the addition of a molecule to a stack provides roughly the same free energy increment regardless of the size of the stack [80–82].

3.4. A Combined Force Matching/MARTINI model

In Section 3.2, we demonstrated that all the FM CG models exhibit incorrect behaviour in aqueous solution. This originated from insolubility arising from very high values for ΔG_{assoc} and ΔG_{hydr} with the wrong sign. To address this, we present a proof-of-concept model which combines CG potentials from force matching and MARTINI 3. This approach is tested in order to improve the poor properties of CG aqueous systems constructed by force matching by combining the solute potentials with a framework which correctly captures the solvent behaviour. The hypothesis here is to examine whether FM potentials can inherently reproduce the reference structures and if this is being hindered by the observed insolubility. This model, PER-FM-M3, utilises potentials from force matching to represent solute–solute interactions but employs MARTINI 3 water and ions as the solvent to describe the solvent–solvent and solute–solvent interactions. Here, electrostatic interactions are treated within the MARTINI 3 framework but the hybrid FM approach, allows solute charges to be treated explicitly, providing a good representation of short-range electrostatics within a chromonic aggregate. Similar approaches have been reported to mix atomistic solutes with MARTINI solvent using virtual sites [83–85] and combining bottom-up CG potentials with MARTINI water [86]. The solute–solute potentials and partial charges are taken from the FM1 model, without modification, and all other interactions are defined by MARTINI 3, as displayed in the interaction matrix for this model (Table 2). All CG potentials were tabulated so that FM potentials have a cutoff of 1.2 nm. MARTINI 3 potentials and cross-interactions used the usual cutoff of 1.1 nm. All other simulation parameters for this model were the same as MARTINI 3. The thermodynamic state points for the simulations are unchanged.

The free energy of association obtained for the PER-FM-M3 model is -115 ± 3 kJ mol^{-1} at a COM distance of 0.36 nm. This binding energy is appreciably higher than the AA and M3 value but shows an improvement compared to the FM models (see Fig. 8(a) for the PMF profile). The hydration free energy calculated is -149 ± 2 kJ mol^{-1}, which is comparable to the AA reference and indicates that this model should be appropriately soluble. The system snapshot in Fig. 8(b) shows that this model exhibits discrete

Table 2
Interaction matrix for the combined force matching/MARTINI model (PER-FM-M3). Bold entries denote potentials obtained from force matching (see Fig. 4(a) for bead definitions), whereas normal entries correspond to MARTINI 3 interactions.

Bead type	C	N	O	Q	W	S
C	**CC**	**CN**	**CO**	**CQ**	TC4/WN	TC4/TQ1
N	–	**NN**	**NO**	**NQ**	P3/WN	P3/TQ1
O	–	–	**OO**	**OQ**	TC3/WN	TC3/TQ1
Q	–	–	–	**QQ**	Qp/WN	Qp/TQ1
W	–	–	–	–	WN/WN	WN/TQ1
S	–	–	–	–	–	TQ1/TQ1

stacks, with the self-assembly behaviour being in good agreement with the AA system and the M3 models. The recovery of the correct self-assembly using the new combined model demonstrates that it is the solvent–solute interactions that are the major weakness in the FM CG models and that the FM potentials for the chromonic mesogen can intrinsically exhibit the correct structures and self-assembly behaviour. For chromonics, we are requiring these potentials to be able to represent a range of aggregation behaviour at a single state point and this is extremely sensitive to thermodynamic, rather than structural properties.

In principle, the optimisation process outlined in Section 3.3 can be applied to the core–water (TC4–WN) interaction (or simply changing the bead type) to better reproduce the thermodynamic properties. While this allows for tuning of the binding energy of the model, the approach is limited as the FM potentials cannot be modified without reparametrisation and so both ΔG_{assoc} and ΔG_{hydr} would have to be optimised through the variation of the solute–solvent interactions alone. It is found that a reduction in the binding energy can be achieved by changing the MARTINI bead types to more hydrophilic/polar definitions, but this concurrently increases the hydration free energy. Thus, the resulting systems have a poorer balance between these properties and the self-assembly into stacks is disrupted, where dimers/trimers are the largest species observed in MD simulations.

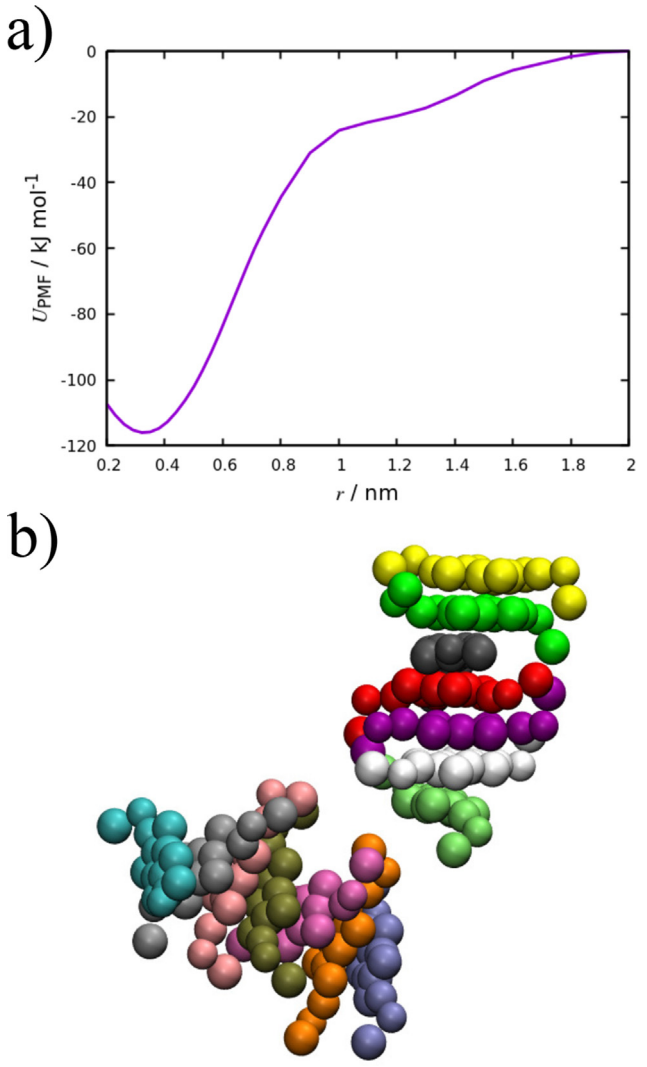

Fig. 8. (a) PMF for a dimer of PER-FM-M3 and (b) a simulation snapshot from a 10 wt% system of 15 molecules with individual molecules coloured differently for clarity.

4. Conclusions

Atomistic simulations of a chromonic perylene dye demonstrate the formation of H-aggregates in water, with a free energy of association in agreement with experimental findings. We have also developed CG models for this chromonic perylene dye and assessed their effectiveness in reproducing the atomistic self-assembly behaviour in terms of the structure of aggregates in aqueous solution and the free energies of association and hydration.

Out-of-the box, a MARTINI 3 model performs extremely well in exhibiting chromonic behaviour and we apply a simple optimisation procedure to tune MARTINI 3 to obtain the exact reproduction of target properties including the association free energy. Using the atomistic simulations as a reference, we also constructed several CG models by a hybrid force matching methodology using a number of strategies to fit the atomistic structures. It is found that the representability of the FM chromonic system can be improved by selecting a more comprehensive reference of configurations in aqueous solution, but all FM models fail to adequately satisfy our assessment criteria. We suggest that enhancements for capturing the correct solubility and response to the local environment could address these limitations.

However, a combined framework using potentials from force matching for the chromonic dye, while using MARTINI 3 to represent the solute–solvent/solvent–solvent interactions, recovers the correct self-assembly behaviour, despite the thermodynamic properties being overestimated. This indicates that the FM method can construct CG potentials which can intrinsically reproduce the AA self-assembly, but the manifestation of this behaviour is hindered by the poor solubility of the models.

Overall, we have demonstrated the strengths and weakness of bottom-up and top-down methodologies for coarse-graining approaches for ionic chromonic liquid crystals and highlighted the challenges in developing successful coarse-grained models for these systems. We suggest that the strategies represented here for chromonics are relevant for improving the coarse-grained modelling of a range of diverse systems in solution. These include conventional lyotropic systems, where self-assembly leads to formation of micelles and lyotropic liquid crystal phases; and proteins, where changes in solvent activity can lead to changes in self-

assembly and/or to changes in shape through changes in protein folding.

Declaration of Competing Interest

The authors declare that they have no known competing financial interests or personal relationships that could have appeared to influence the work reported in this paper.

Acknowledgements

This research was supported by Durham University and EPSRC (EP/R513039/1). The authors would like to thank Durham University for providing computer time on its high performance computer system, Hamilton. The authors would also like to thank Martin Walker and Thomas Potter for their insightful discussions.

Appendix A. Supplementary material

Supplementary data associated with this article can be found, in the online version, at https://doi.org/10.1016/j.molliq.2021.118210.

References

[1] H. Zollinger, Color Chemistry: Synthesis, Properties and Applications of Organic Dyes and Pigments, 3rd Edition., VCH, Weinheim, 2003.
[2] F. Würthner, Perylene bisimide dyes as versatile building blocks for functional supramolecular architectures, Chem. Commun. 14 (2004) 1564–1579.
[3] F. Würthner, C.R. Saha-Möller, B. Fimmel, S. Ogi, P. Leowanawat, D. Schmidt, Perylene bisimide dye assemblies as archetype functional supramolecular materials, Chem. Rev. 116 (2016) 962–1052.
[4] C. Huang, S. Barlow, S.R. Marder, Perylene-3,4,9,10-tetracarboxylic acid diimides: Synthesis, physical properties, and use in organic electronics, J. Org. Chem. 76 (2011) 2386–2407.
[5] A. Nowak-Król, F. Würthner, Progress in the synthesis of perylene bisimide dyes, Org. Chem. Front 6 (2019) 1272–1318.
[6] I.K. Iverson, S.-W. Tam-Chang, Cascade of molecular order by sequential self-organization, induced orientation, and order transfer processes, J. Am. Chem. Soc. 121 (1999) 5801–5802.
[7] S.-W. Tam-Chang, W. Seo, K. Rove, S.M. Casey, Molecularly designed chromonic liquid crystals for the fabrication of broad spectrum polarizing materials, Chem. Mater. 16 (2004) 1832–1834.
[8] S.-W. Tam-Chang, W. Seo, I.K. Iverson, Synthesis and studies of the properties of a liquid-crystalline quaterrylenebis(dicarboximide) by 1H NMR and UV-vis spectroscopies, J. Org. Chem. 69 (2004) 2719–2726.
[9] S.-W. Tam-Chang, J. Helbley, T.D. Carson, W. Seo, I.K. Iverson, Template-guided organization of chromonic liquid crystals into micropatterned anisotropic organic solids, Chem. Commun. 5 (2006) 503–505.
[10] S.-W. Tam-Chang, L. Huang, Chromonic liquid crystals: properties and applications as functional materials, Chem. Commun. 17 (2008) 1957–1967.
[11] C. Rodríguez-Abreu, C. Aubery-Torres, C. Solans, A. Lopez-Quintela, G.J.T. Tiddy, Characterization of perylene diimide dye self-assemblies and their use as templates for the synthesis of hybrid and supermicroporous nanotubules, ACS Appl. Mater. Interfaces 3 (2011) 4133–4141.
[12] J. Lydon, Chromonic review, J. Mater. Chem. 20 (2010) 10071–10099.
[13] I.K. Iverson, S.M. Casey, W. Seo, S.-W. Tam-Chang, Controlling molecular orientation in solid films via self-organization in the liquid-crystalline phase, Langmuir 18 (2002) 3510–3516.
[14] S.-W. Tam-Chang, I.K. Iverson, J. Helbley, Study of the chromonic liquid-crystalline phases of bis-(N, N-diethylaminoethyl)perylene-3,4,9,10-tetracarboxylic diimide dihydrochloride by polarized optical microscopy and 2h NMR spectroscopy, Langmuir 20 (2004) 342–347.
[15] T. Ogolla, P.J. Collings, Assembly structure and free energy change of a chromonic liquid crystal formed by a perylene dye, Liq. Cryst. 46 (2019) 1551–1557.
[16] Z. Chen, B. Fimmela, F. Würthner, Solvent and substituent effects on aggregation constants of perylene bisimide π-stacks - a linear free energy relationship analysis, Org. Biomol. Chem. 10 (2012) 5845–5855.
[17] J. Baz, N. Hansen, Thermodynamic characterization of the dimerization of an anionic perylene bisimide dye using molecular simulation, J. Phys. Chem. C 123 (2019) 8027–8036.
[18] K. Bag, R. Halder, B. Jana, S. Malik, Solvent-assisted enhanced emission of cationic perylene diimide supramolecular assembly in water: A perspective from experiment and simulation, J. Phys. Chem. C 123 (2019) 6241–6249.
[19] G. Yu, M. Walker, M.R. Wilson, Atomistic simulation studies of ionic cyanine dyes: self-assembly and aggregate formation in aqueous solution, Phys. Chem. Chem. Phys. 23 (2021) 6408–6421.
[20] F. Chami, M.R. Wilson, Molecular order in a chromonic liquid crystal: a molecular simulation study of the anionic azo dye sunset yellow, J. Am. Chem. Soc. 132 (2010) 7794–7802.
[21] A. Akinshina, M. Walker, M.R. Wilson, G.J.T. Tiddy, A.J. Masters, P. Carbone, Thermodynamics of the self-assembly of non-ionic chromonic molecules using atomistic simulations. the case of TP6EO2M in aqueous solution, Soft Matter 11 (2015) 680–691.
[22] R. Thind, M. Walker, M.R. Wilson, Molecular simulation studies of cyanine-based chromonic mesogens: Spontaneous symmetry breaking to form chiral aggregates and the formation of a novel lamellar structure, Adv. Theory Simul. 1 (2018) 1800088.
[23] O.M.M. Rivas, A.D. Rey, Molecular dynamics on the self-assembly of mesogenic graphene precursors, Carbon 110 (2016) 189–199.
[24] O.M.M. Rivas, A.D. Rey, Molecular dynamics of dilute binary chromonic liquid crystal mixtures, Mol. Syst. Des. Eng. 2 (2017) 223–234.
[25] O.M.M. Rivas, A.D. Rey, Effects of sodium and magnesium cations on the aggregation of chromonic solutions using molecular dynamics, J. Phys. Chem. B 123 (2019) 1718–1732.
[26] O.M.M. Rivas, A.D. Rey, Molecular dynamics study of the effect of l-alanine chiral dopants on diluted chromonic solutions, J. Phys. Chem. B 123 (2019) 8995–9010.
[27] F. Haverkort, A. Stradomska, A.H. de Vries, J. Knoester, Investigating the structure of aggregates of an amphiphilic cyanine dye with molecular dynamics simulations, J. Phys. Chem. B 117 (2013) 5857–5867.
[28] F. Haverkort, A. Stradomska, J. Knoester, First-principles simulations of the initial phase of self-aggregation of a cyanine dye: structure and optical spectra, J. Phys. Chem. B 118 (2014) 8877–8890.
[29] C. Friedl, T. Renger, H. von Berlepsch, K. Ludwig, M.S. am Busch, J. Megow, Structure prediction of self-assembled dye aggregates from cryogenic transmission electron microscopy, molecular mechanics, and theory of optical spectra, J. Phys. Chem. C 120 (2016) 19416–19433.
[30] E. Brini, E.A. Algaer, P. Ganguly, C. Li, F. Rodriguez-Ropero, N.F. van der Vegt, Systematic coarse-graining methods for soft matter simulations - a review, Soft Matter 9 (2013) 2108–2119.
[31] M. Walker, A.J. Masters, M.R. Wilson, Self-assembly and mesophase formation in a non-ionic chromonic liquid crystal system: insights from dissipative particle dynamics simulations, Phys. Chem. Chem. Phys. 16 (2014) 23074–23081.
[32] M. Walker, M.R. Wilson, Formation of complex self-assembled aggregates in non-ionic chromonics: dimer and trimer columns, layer structures and spontaneous chirality, Soft Matter 12 (2016) 8588–8594.
[33] T.D. Potter, J. Tasche, E.L. Barrett, M. Walker, M.R. Wilson, Development of new coarse-grained models for chromonic liquid crystals: insights from top-down approaches, Liq. Cryst. 44 (2017) 1979–1989.
[34] T.D. Potter, M. Walker, M.R. Wilson, Self-assembly and mesophase formation in a non-ionic chromonic liquid crystal: insights from bottom-up and top-down coarse-grained simulation models, Soft Matter 16 (2020) 9488–9498.
[35] S. Izvekov, G.A. Voth, A multiscale coarse-graining method for biomolecular systems, J. Phys. Chem. B 109 (2005) 2469–2473.
[36] P. Liu, S. Izvekov, G.A. Voth, Multiscale coarse-graining of monosaccharides, J. Phys. Chem. B 111 (2007) 11566–11575.
[37] V. Rühle, C. Junghans, Hybrid approaches to coarse-graining using the VOTCA package: Liquid hexane, Macromol. Theory Simul. 20 (2011) 472–477.
[38] P.C.T. Souza, R. Alessandri, J. Barnoud, S. Thallmair, I. Faustino, F. Grünewald, I. Patmanidis, H. Abdizadeh, B.M.H. Bruininks, T.A. Wassenaar, P.C. Kroon, J. Melcr, V. Nieto, V. Corradi, H.M. Khan, J. Domański, M. Javanainen, H. Martinez-Seara, N. Reuter, R.B. Best, I. Vattulainen, L. Monticelli, X. Periole, D.P. Tieleman, A.H. de Vries, S.J. Marrink, Martini 3: a general purpose force field for coarse-grained molecular dynamics, Nat. Methods 18 (2021) 382–388.
[39] J. Wang, R.M. Wolf, J.W. Caldwell, P.A. Kollman, D.A. Case, Development and testing of a general Amber force field, J. Comput. Chem. 25 (2004) 1157–1174.
[40] J. Wang, W. Wang, P.A. Kollman, D.A. Case, Automatic atom type and bond type perception in molecular mechanical calculations, J. Mol. Graph. Model. 25 (2006) 247–260.
[41] A. Jakalian, D.B. Jack, C.I. Bayly, Fast, efficient generation of high-quality atomic charges. AM1-BCC model: II. parameterization and validation, J. Comput. Chem. 23 (2002) 1623–1641.
[42] A.W.S. da Silva, W.F. Vranken, ACPYPE - AnteChamber PYthon Parser interfacE, BMC Res. Notes 5 (2012) 367.
[43] W.L. Jorgensen, J. Chandrasekhar, J.D. Madura, R.W. Impey, M.L. Klein, Comparison of simple potential functions for simulating liquid water, J. Chem. Phys. 79 (1983) 926–935.
[44] B. Jójárt, T.A. Martinek, Performance of the general Amber force field in modeling aqueous popc membrane bilayers, J. Comput. Chem. 28 (2007) 2051–2058.
[45] S. Pronk, S. Páll, R. Schulz, P. Larsson, P. Bjelkmar, R. Apostolov, M.R. Shirts, J.C. Smith, P.M. Kasson, D. van der Spoell, B. Hess, E. Lindahl, GROMACS 4.5: a high-throughput and highly parallel open source molecular simulation toolkit, Bioinformatics 29 (2013) 845–854.
[46] U. Essmann, L. Perera, M.L. Berkowitz, T. Darden, H. Lee, L.G. Pedersen, A smooth particle mesh ewald method, J. Chem. Phys. 103 (1995) 8577–8593.
[47] H.J.C. Berendsen, J.P.M. Postma, W.F. van Gunsteren, A. DiNola, J.R. Haak, Molecular dynamics with coupling to an external bath, J. Chem. Phys. 81 (1984) 3684–3690.
[48] S. Nosé, A unified formulation of the constant temperature molecular dynamics methods, J. Chem. Phys. 81 (1984) 511–519.

[49] W.G. Hoover, Canonical dynamics: Equilibrium phase-space distributions, Phys. Rev. A 31 (1985) 1695–1697.
[50] M. Parrinello, A. Rahman, Polymorphic transitions in single crystals: A new molecular dynamics method, J. Appl. Phys. 52 (1981) 7182–7190.
[51] B. Hess, H. Bekker, H.J.C. Berendsen, J.G.E.M. Fraaije, LINCS: A linear constraint solver for molecular simulations, J. Comput. Chem. 18 (1997) 1463–1472.
[52] D.H. de Jong, S. Baoukina, H.I. Ingólfsson, S.J. Marrink, Martini straight: Boosting performance using a shorter cutoff and GPUs, Comput. Phys. Commun. 199 (2016) 1–7.
[53] G. Bussi, D. Donadio, M. Parrinello, Canonical sampling through velocity rescaling, J. Chem. Phys. 126 (2007) 014101.
[54] J.A. Barker, R.O. Watts, Monte carlo studies of the dielectric properties of water-like models, Mol. Phys. 26 (1973) 789–792.
[55] F. Ercolessi, J.B. Adams, Interatomic potentials from first-principles calculations: The force-matching method, Europhys. Lett. 26 (1994) 583–588.
[56] W.G. Noid, J.W. Chu, G.S. Ayton, V. Krishna, S. Izvekov, G.A. Voth, A. Das, H.C. Andersen, The multiscale coarse-graining method. I. a rigorous bridge between atomistic and coarse-grained models, J. Chem. Phys. 128 (2008) 244114.
[57] W.G. Noid, P. Liu, Y. Wang, J.W. Chu, G.S. Ayton, S. Izvekov, H.C. Andersen, G.A. Voth, The multiscale coarse-graining method. II. numerical implementation for coarse-grained molecular models, J. Chem. Phys. 128 (2008) 244115.
[58] L. Lu, S. Izvekov, A. Das, H.C. Andersen, G.A. Voth, Efficient, regularized, and scalable algorithms for multiscale coarse-graining, J. Chem. Theory Comput. 6 (2010) 954–965.
[59] N.J.H. Dunn, K.M. Lebold, M.R. DeLyser, J.F. Rudzinski, W.G. Noid, BOCS: Bottom-up open-source coarse-graining software, J. Phys. Chem. B 122 (2018) 3363–3377.
[60] T.D. Potter, J. Tasche, M.R. Wilson, Assessing the transferability of common top-down and bottom-up coarse-grained molecular models for molecular mixtures, Phys. Chem. Chem. Phys. 21 (2019) 1912–1927.
[61] V. Rühle, C. Junghans, A. Lukyanov, K. Kremer, D. Andrienko, Versatile object-oriented toolkit for coarse-graining applications, J. Chem. Theory Comput. 5 (2009) 3211–3223.
[62] S.Y. Mashayak, M.N. Jochum, K. Koschke, N.R. Aluru, V. ühle, C. Junghans, Relative entropy and optimization-driven coarse-graining methods in VOTCA, PLos One 10 (2015) e0131754.
[63] A. Das, H.C. Andersen, The multiscale coarse-graining method. V. isothermal-isobaric ensemble, J. Chem. Phys. 132 (2010) 164106.
[64] N.J.H. Dunn, W.G. Noid, Bottom-up coarse-grained models with predictive accuracy and transferability for both structural and thermodynamic properties of heptane-toluene mixtures, J. Chem. Phys. 144 (2016) 204124.
[65] M.R. DeLyser, W.G. Noid, Extending pressure-matching to inhomogeneous systems via local-density potentials, J. Chem. Phys. 147 (2017) 134111.
[66] S.J. Marrink, H.J. Risselada, S. Yefimov, D.P. Tieleman, A.H. de Vries, The MARTINI force field: Coarse grained model for biomolecular simulations, J. Chem. Phys. B 111 (2007) 7812–7824.
[67] L. Monticelli, S.K. Kandasamy, X. Periole, R.G. Larson, D.P. Tieleman, S.J. Marrink, The MARTINI coarse-grained force field: Extension to proteins, J. Chem. Theory Comput. 4 (2008) 819–834.
[68] D.H. de Jong, G. Singh, W.F.D. Bennett, C. Arnarez, T.A. Wassenaar, L.V. Schäfer, X. Periole, D.P. Tieleman, S.J. Marrink, Improved parameters for the martini coarse-grained protein force field, J. Chem. Theory Comupt. 9 (2013) 687–697.
[69] Martini 3 open beta. [link]. http://cgmartini.nl/index.php/martini3beta.
[70] A. Villa, C. Peter, N.F.A. van der Vegt, Self-assembling dipeptides: conformational sampling in solvent-free coarse-grained simulation, Phys. Chem. Chem. Phys. 11 (2009) 2077–2086.
[71] A. Villa, N.F.A. van der Vegt, C. Peter, Self-assembling dipeptides: including solvent degrees of freedom in a coarse-grained model, Phys. Chem. Chem. Phys. 11 (2009) 2068–2076.
[72] C. Li, J. Shen, C. Peter, N.F.A. van der Vegt, A chemically accurate implicit-solvent coarse-grained model for polystyrenesulfonate solutions, Macromolecules 45 (2012) 2551–2561.
[73] C.H. Bennett, Efficient estimation of free energy differences from Monte Carlo data, J. Comput. Phys. 22 (1976) 245–268.
[74] J.W. Mullinax, W.G. Noid, Extended ensemble approach for deriving transferable coarse-grained potentials, J. Chem. Phys. 131 (2009) 104110.
[75] N.J.H. Dunn, W.G. Noid, Bottom-up coarse-grained models with predictive accuracy and transferability for both structural and thermodynamic properties of heptane-toluene mixtures, J. Chem. Phys. 144 (2016) 204124.
[76] H. Wang, C. Junghans, K. Kremer, Comparative atomistic and coarse-grained study of water: What do we lose by coarse-graining?, Eur Phys. J. E 28 (2009) 221–229.
[77] T. Sanyal, M.S. Shell, Coarse-grained models using local-density potentials optimized with the relative entropy: Application to implicit solvation, J. Chem. Phys. 145 (2016) 034109.
[78] T. Sanyal, M.S. Shell, Transferable coarse-grained models of liquid-liquid equilibrium using local density potentials optimized with the relative entropy, J. Phys. Chem. B 122 (2018) 5678–5693.
[79] J. Jin, G.A. Voth, Ultra-coarse-grained models allow for an accurate and transferable treatment of interfacial systems, J. Chem. Theory Comput. 14 (2018) 2180–2197.
[80] J.R. Henderson, Concentration dependence of linear self-assembly and exactly solvable models, Phys. Rev. Lett. 77 (1996) 2316–2319.
[81] J.R. Henderson, Physics of isodesmic chemical equilibria in solution, Phys. Rev. E 55 (1997) 5731–5742.
[82] J.R. Henderson, Linear aggregation beyond isodesmic symmetry, J. Chem. Phys. 130 (2009) 45101–45103.
[83] A.J. Rzepiela, M. Louhivuori, C. Peter, S.J. Marrink, Hybrid simulations: combining atomistic and coarse-grained force fields using virtual sites, Phys. Chem. Chem. Phys. 13 (2011) 10437–10448.
[84] T.A. Wassenaar, H.I. Ingólfsson, M. Prieß, S.J. Marrink, L.V. Schäfer, Mixing MARTINI: Electrostatic coupling in hybrid atomistic-coarse-grained biomolecular simulations, J. Phys. Chem. B 117 (2013) 3516–3530.
[85] S. Genheden, Solvation free energies and partition coefficients with the coarse-grained and hybrid all-atom/coarse-grained martini models, J. Comput. Aided Mol. Des. 31 (2017) 867–876.
[86] K. Prasitnok, M.R. Wilson, A coarse-grained model for polyethylene glycol in bulk water and at a water/air interface, Phys. Chem. Chem. Phys. 15 (2013) 17093–17104.